

Ultra-high temperature HfB₂–SiC ceramics consolidated by hot-pressing and spark plasma sintering

Frédéric Monteverde*

Institute of Science and Technology for Ceramics, National Research Council, Via Granarolo 64, I-48018 Faenza, Italy

Received 8 November 2005; accepted 24 January 2006

Available online 27 June 2006

Abstract

Two ultra-high temperature HfB₂–SiC ceramics were successfully consolidated by hot-pressing (HP) and spark plasma sintering (SPS). The powder mixture HfB₂ + 30 vol% SiC was brought to full densification with the addition of 2 vol% TaSi₂ as sintering aid, and applying the following conditions: 2100 °C for 3 min (SPS), or 1900 °C for 35 min (HP). The microstructure consisted of regular micrometric diboride grains and SiC particles homogeneously distributed. The major secondary phases were HfO₂, and (Ta, Hf)-mixed or Hf carbides in the materials processed by SPS and HP, respectively. Both SiC and TaSi₂ beneficially contributed to boost the sinterability of HfB₂ at elevated temperatures.

The mechanical properties showed interesting potential. Elastic moduli above 490 GPa were measured. Flexural strengths at room temperature and 1500 °C (in air) of the hot-pressed composite were 665 ± 75 and 480 ± 30 MPa, respectively. Machining-induced flaws rather than fabrication defects adversely affected the room temperature strength of the spark plasma sintered material, leading to premature failure. The steep cooling up to 1000 °C in about 2 min associated to SPS induced large unrelaxed thermal stresses, which enhanced the tendency to micro-cracking during machining. However, such a strained configuration had a beneficial effect on fracture toughness.

In the temperature range of 1450–1650 °C both the as-fired materials tolerated acceptably the oxidation attack in air. Thermo-gravimetric tests at 1450 °C for 20 h had mass gains of 4.10 ± 0.02 and 3.30 ± 0.02 mg/cm² for the materials processed by HP and SPS, respectively, and decelerating kinetics were recorded, although not conclusively parabolic.

© 2006 Elsevier B.V. All rights reserved.

Keywords: HfB₂; Spark plasma sintering; Microstructure; Mechanical properties; Oxidation resistance

1. Introduction

Thermal protection structures with superior properties are needed for the next generation of (hypersonic) re-entry space vehicles which, when equipped with sharp aerosurfaces like wing leading edges or nose-caps, have projected requirements for materials operating at temperatures above 2000 °C in both neutral and oxidising environments [1]. Ultra-high temperature ceramics (UHTCs) are a group of materials that have melting temperatures above 3000 °C, and that have shown some potentials for such applications [2]. In addition to uses in aerospace, UHTCs are currently applied in a variety of high-temperature structural applications including engines, plasma-arc electrodes, molten metal crucibles, cutting tools, and wear-resistant coatings.

Historically, ZrB₂- and HfB₂-based materials have been the choice for high-temperature ablation resistant applications in oxidising atmosphere. This couple of borides is appealing, thanks to their melting points (i.e. 3245 °C for ZrB₂ and 3380 °C for HfB₂), and to the capacity of forming protective oxidation-resistant scales in use at elevated temperatures.

Hot-pressing (HP) has been the widely used sintering technique for producing highly dense UHTCs. The addition of SiC to MB₂ (M = Hf or Zr), due to its excellent refractoriness, has been looked at for the fabrication of best-performing MB₂–SiC ceramics with enhanced thermo-mechanical capabilities [2]. In the continuing pursuit to obtain improved UHTCs, additives were utilised in order to develop desired microstructures which are key in the control of the material performances [3–5].

Spark plasma sintering (SPS) has emerged as a non-conventional powder consolidation method in densifying a number of poorly sinterable ceramics in very short times [6]. In this technique, densification is stimulated by the application of

* Tel.: +39 0546 699758; fax: +39 0546 46381.

E-mail address: fmonte@istec.cnr.it.

a pulsed electric field, combined with resistance heating and pressure. Several experiments emphasised that high-rate and possibly low-temperature sintering are indeed characteristics of this technique.

Central goal of the present study is to compare densification, microstructures, thermo-mechanical properties, and resistance to oxidation of an HfB₂–30 vol% SiC composition, modified by 2 vol% TaSi₂ and processed either by SPS and by HP.

2. Experimental

2.1. Powder processing and sintering

An HfB₂–SiC commercial powder mixture was ball-milled in ethyl alcohol for 48 h, using high-purity SiC milling media. TaSi₂ was separately dispersed in ethyl alcohol using a pulsed sonicator (20 min total time) coupled with a magnetic stirring, poured into the ball-milled HfB₂–SiC slurry and then re-sonicated (30 min total time) under continuous magnetic stirring. After drying in a rotating evaporator flushing argon continuously, the powder mixture was sieved through a 250 µm mesh screen. Table 1 shows characteristics and proportions of the raw powders used.

Next, the powder mixture was processed using an SPS furnace (FCT Systeme GmbH, Rauenstein, Germany) once the loose powders, pre-compacted into a graphite die (i.d. 40 mm, lined with a 0.75 mm thick graphitised paper) were further installed inside the SPS furnace chamber. The following parameters were set: ≈0.1 mbar terminal chamber pressure, 100 °C/min heating rate, 2100 °C final set-point, and 3 min dwell time. The uniaxial mechanical pressure of 30 MPa was applied through graphite punches from the start of the heating ramp to the end of the dwell time. The pressure was then released, and the sample rapidly cooled down by flushing nitrogen inside the SPS furnace chamber. The temperature was measured by an optical pyrometer focused on the bottom of the upper graphite punch, about 4 mm from the sample. Shrinkage of the powder compact was recorded with a linear gauge. The corresponding data were corrected for thermal expansion of the graphite punches. This material produced by SPS will be referred to as HST_SPS. An additional SPS test (thereafter labelled HS_SPS) was performed at the same processing conditions using the ball-milled HfB₂–30 vol% SiC powder free of TaSi₂.

The HfB₂–SiC–TaSi₂ powder mixture was also hot-pressed at low vacuum (0.5 mbar) using an inductively heated graphite die lined with a BN-sprayed graphitised 0.75 mm-thick foil. The peak temperature (measured with a pyrometer focused on the graphite die) and the dwell time were 1900 °C and 35 min, respectively. The external pressures during heating and over the isothermal stage were 30 and 42 MPa, respectively. Linear shrinkage of the sample was recorded by measuring the displacement of rams. This material produced by hot-pressing will be referred to as HST_HP.

2.2. Material's characterization and oxidation tests

2.2.1. Microstructure

Densities of the as-fired specimens were obtained using the Archimedes' immersion method. The phase composition was analysed with an X-ray diffractometer (XRD, Ni-filtered Cu Kα radiation, mod. D500, Siemens, Germany)

Table 1
Characteristics and proportions (vol%) of the commercial powders used

Powder	Company	vol%	Type	Particle size	Impurity (wt%)
HfB ₂	Cerac Inc., USA	68	325 mesh	1.7 µm ^a	Zr 0.4
SiC	H.C. Starck, Germany	30	BF 12	11.6 m ² /g ^b	O 0.9
TaSi ₂	ABCR & Co., KG, Germany	2	325 mesh	<10 µm	–

^a Fisher size (APS).

^b Specific surface area.

and a scanning electron microscope (SEM, mod. S360, Leica Cambridge, UK) equipped with an energy dispersive X-ray microanalyser (EDX, mod. INCA Energy 300, Oxford Instruments, UK). Cross-sections were polished with diamond-based pastes to 0.25 µm. Fracture and polished surfaces were imaged by SEM using secondary electrons (SEs).

2.2.2. Thermo-mechanical properties

The Young's modulus (E) and Poisson's ratio (ν) were measured on 28 mm × 8 mm × 0.8 mm specimens by the resonance frequency method in bending using an H&P gain-phase analyser. Flexural strength (σ) was tested at room temperature (five specimens) and at 1500 °C (three specimens) in ambient air on chamfered bars of dimensions 25 mm × 2.5 mm × 2 mm (length × width × thickness, respectively). The strength tests were performed on a semi-articulated SiC 4-pt jig with a lower span of 20 mm and an upper span of 10 mm on an universal screw-type testing machine (Instron 6028), using a cross-head speed of 0.5 mm/min. For the high-temperature tests, a hold of 18 min was awaited to allow thermal equilibrium. Fracture toughness (K_{Ic}) was measured by the chevron-notched-beam method at room temperature (three specimens) using 25 mm × 2 mm × 2.5 mm (length × width × thickness, respectively) bars on the same jig used for the flexural strength (cross-head speed 0.05 mm/min). The thermal expansion up to 1300 °C was evaluated using a dilatometer (mod. DIL 402E, NETZSCH Gerätebau GmbH, Germany) in a stream of argon, 5 °C/min heating rate.

2.2.3. Resistance to oxidation

The resistance to oxidation was tested in various conditions.

- (OX1) Temperature range of 1450–1650 °C in stagnant air, exposure of 1 h and coupons of dimensions 12.5 mm × 2.5 mm × 2 mm.
- (OX2) At 1650 and 1700 °C, exposure of 5 min, test bars of dimensions 25 mm × 2.5 mm × 2 mm
- (OX3) At 1450 °C for 20 h in flowing dry air (15 cm³/min), 30 °C/min of heating rate and free cooling, using a thermo-gravimetric analyser (mod. STA449 Jupiter, NETZSCH Gerätebau GmbH, Germany), equipped with a vertically heated Al₂O₃ chamber. Spacers of zirconia were placed between the specimen (dimensions 12.5 mm × 2.5 mm × 2 mm) and the Al₂O₃ holder with minimal contact area.

All the tested specimens were first cleaned in acetone, and then kept at 80 °C for 2 h. Mass of the specimens was measured before and after exposure. The microstructural modifications induced in the oxidised specimens were evaluated by SEM–EDX observing the corresponding cross-sections, which were polished to 0.25 µm using non-aqueous lubricants in order to preserve any boron-containing glass species.

For the conditions OX1 and OX2, once the specimens had been slotted upon SiC supports into the bottom-loading furnace box (MoSi₂ heating elements), the highest furnace temperature was reached within 1 min. The specimens were then air-quenched after the hold.

The 4-pt. residual flexural strength of the test bars exposed at 1650 or 1700 °C (condition OX2) was measured at room temperature (three specimens tested), according to the conditions aforementioned.

3. Results

3.1. Densification and microstructure development

The densification curves during SPS and HP are shown in Figs. 1 and 2, respectively. The different heating rates of the two sintering techniques implied an entire duration (cooling excluded) of about 23 min for SPS and 140 min for HP. The peak temperature of 2100 °C for HST_SPS was set once the densification rate appeared to rapidly fall down. For comparison, the densification curve of HS_SPS (the silicide-free HfB₂–30SiC composition) is shown in Fig. 1. The onsets of some measurable shrinkage for HST_SPS and HST_HP were at around 1300 and

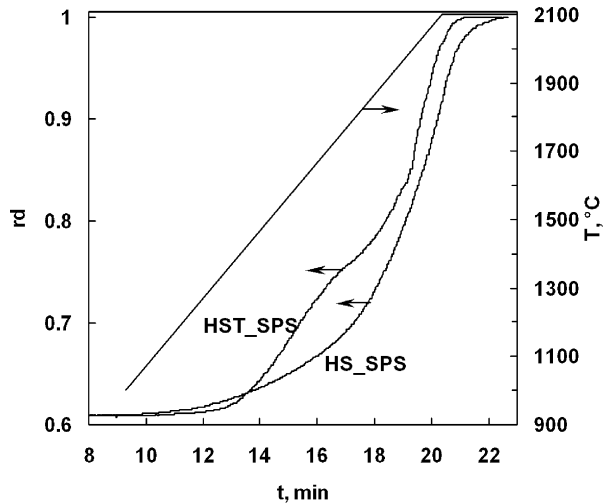


Fig. 1. Relative density (rd) vs. time (t) or temperature (T) of HST_SPS and HS_SPS.

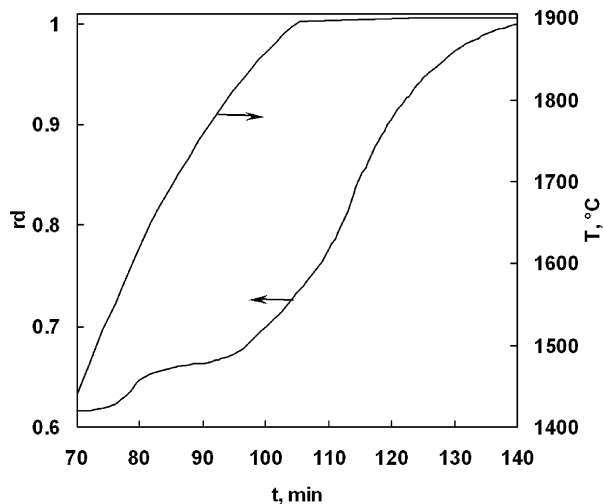


Fig. 2. Relative density (rd) vs. time (t) or temperature (T) of HST_HP.

1520 °C, respectively. In Fig. 2, the weakly increasing section in the densification curve of HST_HP from 1700 up to 1830 °C did not find an adequate correspondence in the densification curve of HST_SPS, but was replaced by a more obvious increasing pattern.

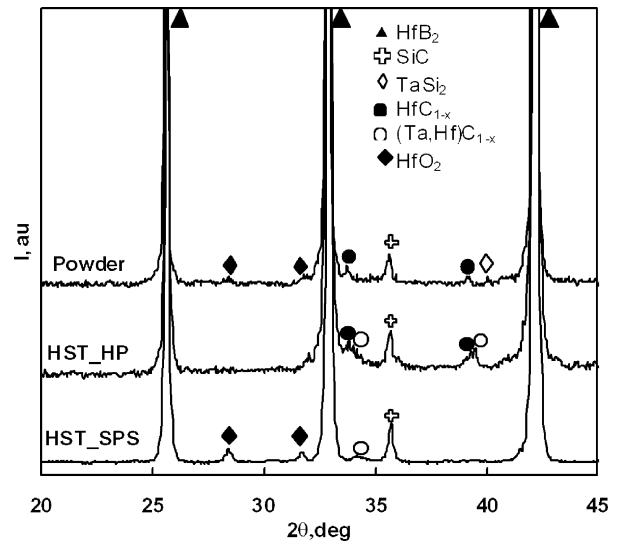


Fig. 4. XRD patterns of the starting powder mixture, and of the as-fired HST_HP and HST_SPS materials.

The bulk densities of the as-sintered materials were 8.66 and 8.62 gr/cm³ for HST_SPS and HST_HP, respectively. Examples of the typical grained structure of the ceramics are given in Fig. 3, the average grain size of HST_SPS being greater than that of HST_HP. Polished sections observed by SEM did not provide evidence of residual porosity in appreciable amounts.

In Fig. 4, the XRD patterns of the starting HfB₂–SiC–TaSi₂ powder mixture, and of the as-fired materials are shown. The main components HfB₂ and SiC apart, some compounds in limited amounts were identified. TaSi₂ disappeared in the sintered HST_HP and HST_SPS compacts, and gave rise to phases compatible to cubic carbides.

The examination of polished sections by SEM–EDX (Fig. 5) highlighted the chemical nature of the newly formed compounds. They consist of Ta-based carbides whose (cubic) lattice incorporated Hf atoms. Some of the larger ones are clearly visible in correspondence of clustered formations. Such features, often enclosed by SiC particulates with an irregular shape, grew faster than the remanent diboride matrix. Metal carbides are known to have growing rate higher than the corresponding diborides at elevated temperatures [7]. The clustered formations are believed to derive from the TaSi₂

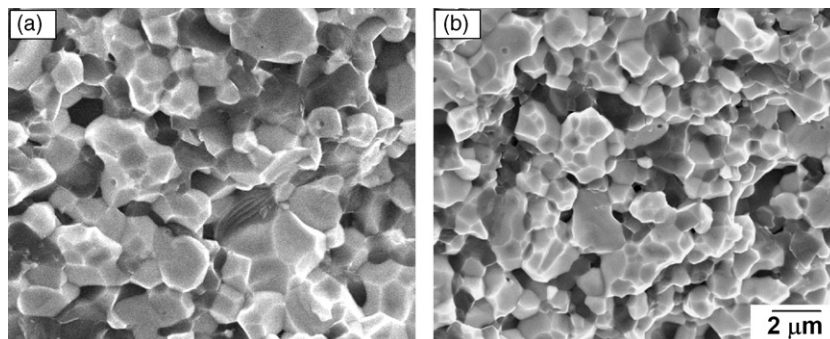


Fig. 3. SE-SEM micrographs from HST_SPS (a) and HST_HP (b): fracture surfaces.

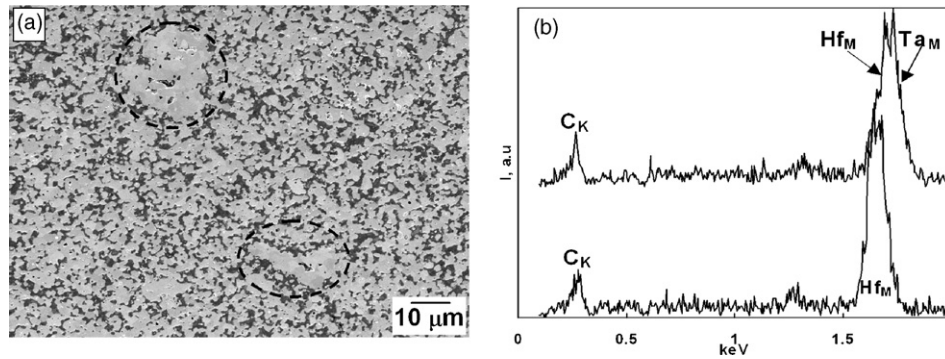


Fig. 5. SE-SEM micrograph from HST_HP: examples of clustered (Ta, Hf)-mixed carbides (a); EDX spectra from Hf-mixed or (Ta, Hf)-mixed carbides (b).

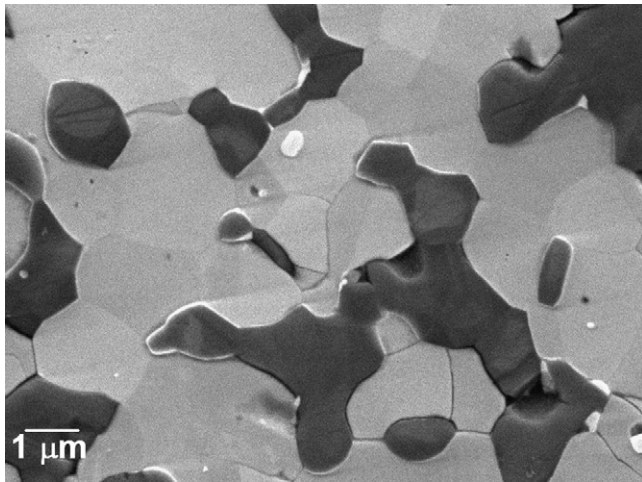


Fig. 6. SE-SEM micrograph from HST_SPS (polished section): the micro-cracking.

raw powder which, though ultrasonically mixed, remained to some extent in hard agglomerates inside the ball-milled HfB_2 -SiC base mixture. The processing time associated to the HP cycle, much longer than that for the SPS cycle, favored the carbo-thermal reduction of HfO_2 into Hf- or (Hf,Ta)-carbides (Fig. 5).

The SiC particulates are homogeneously distributed within the diboride skeleton. Aside from limited pull-outs of some diboride grains, residual inter/intra-granular micro-cracking was observed, mostly in HST_SPS (Fig. 6).

3.2. Thermo-mechanical properties

Table 2 summarizes the experimental data for the measured thermo-mechanical properties. No published values for analogous HfB_2 -SiC-TaSi₂ systems are available to date. The thermal expansion showed a basically linear pattern up to 1300 °C, whilst elastic moduli in excess of 490 GPa were measured.

Flexural strength of HST_HP tested in air at 1500 °C, 480 ± 35 MPa, had a decrease of about 28%, compared to that at room temperature, 665 ± 75 MPa. The additional hold of 1 h at 1500 °C before testing did not cause any further strength penalization.

As far as the HST_SPS material is concerned, the scattering of the strength data was large. On the one hand, the fractographic study in conjunction to the lowest values did not reveal the presence of fabrication defects (for instance, the clustered formations of carbides) as critical as to justify such a decrease. On the other hand, chipped regions on the machined specimens surfaces were seen, and appeared like craters a few tenths μm -wide. Therefore, such a strength drop was attributed to the mechanical machining which stimulated the tendency of this material to micro-cracking, introducing extensive damage on the machined surfaces of the bars. However, magnitude and dispersion of the fracture toughness data, compared to HST_HP, increased. An explanation will be put forward in the discussion.

3.3. The resistance to oxidation

The 1 h exposure data of mass change (w) from 1450 up to 1650 °C, and the Arrhenius plot for extrapolated parabolic

Table 2
Thermo-mechanical properties: Young's modulus, E ; Poisson's ratio, ν ; coefficient of thermal expansion, CTE; fracture toughness, K_{Ic} , and flexural strength, σ at room temperature (RT) and 1500 °C

Material	E (GPa; uncertainty)	ν	CTE ($10^{-6}/^\circ\text{C}$) (25–1300) °C	K_{Ic} (MPa $\sqrt{\text{m}}$, mean \pm 1S.D.) RT	σ (MPa)				
					RT		1500 °C		
					Maximum	(Mean \pm 1S.D.)	Minimum	(Mean \pm 1S.D., no additional hold)	(Mean \pm 1S.D., 1 h additional exposure to air)
HST_HP	489 ± 4	0.088	–	3.6 ± 0.5	730	665 ± 75	590	480 ± 35	490 ± 25
HST_SPS	506 ± 4	0.121	6.95	4.65 ± 0.05	640	465 ± 225	135	–	–

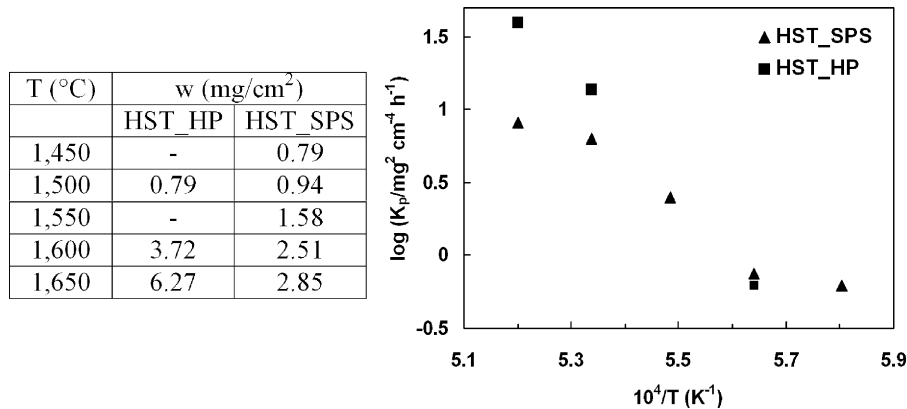


Fig. 7. Mass gains w (± 0.02 mg/cm²) for 1 h exposure in static air at different temperatures. The calculated parabolic rate constants K_P ($K_P = w^2/t$, t the time) are plotted in the Arrhenius graph.

rate constants K_P ($K_P = w^2/t$, t the time) are shown in Fig. 7. The graphical layout of $\log(K_P)$ data for HST_HP appears to fit a parabolic law in the temperature range of 1500–1650 °C whereas, for HST_SPS, it tends to depart from a parabolic pattern above 1600 °C. Within the temperature range tested, HST_SPS had mass gains lower than those of HST_HP: smaller mass gains can be comparatively considered an indication for a higher resistance to oxidation. Opila et al. reported that an $\text{HfB}_2 + 20\text{SiC} + 20\text{TaSi}_2$ composite (vol%), hot-pressed at 1700 °C for 2 h and then oxidised in air at 1627 °C, exhibited parabolic kinetics, being $\log(K_P/\text{mg}^2 \text{cm}^{-4} \text{h}^{-1}) = 0.758$ [8].

Only for HST_SPS, the residual flexural strengths at room temperature of specimens exposed for 5 min to air at 1650 or 1700 °C were (mean \pm 1 S.D.) 435 ± 30 and 310 ± 40 MPa, respectively. An interesting feature is the reduced dispersion of data, compared to that obtained at room temperature on the as-fired material.

The graphical trends of mass gain (w) versus time over the 20 h exposure at 1450 °C are plotted in Fig. 8a: the final mass gains were 4.1 ± 0.02 and 3.3 ± 0.02 mg/cm² for HST_HP and HST_SPS, respectively. Offsets equal to 0.25 ± 0.02 and 0.31 ± 0.02 mg/cm², which accounted for the oxidation preceding the fixed exposure of HST_HP and HST_SPS, respectively, were subtracted from the raw data. The thermo-gravimetric test on the additive-free HS_SPS material using the same testing parameters is included in Fig. 8a for

comparison (final mass gain 0.76 ± 0.02 mg/cm²). A data analysis was carried out using a dummy parabolic rate constant K_D for each mass gain datum (Fig. 8b), assuming $K_D = w^2/t$, t the time. The trend of the $\log(K_D)$ curves indicates that at 1450 °C the oxidation kinetics of HST_SPS and HST_HP on the whole were decelerating, but did not fit properly a parabolic law.

The obvious departure from parabolic kinetics, chiefly during the early stages of the isothermal hold, can be better understood looking at the irregular trend of the $\log(K_D)$ data in Fig. 8b. During the initial exposure, even though net mass gains were dominant, mass loss mechanisms were active as well. Thus, a more effective protection against oxidation was established only for longer exposures. It is proper mentioning that purely parabolic kinetics should have implied constant values of $\log(K_D)$: mass gains of HS_SPS for instance, basically obeyed a parabolic law for exposure above 100 min.

The microstructures of all the oxidised samples generally revealed an external oxide scale characterised by a layered configuration. Such an oxide scale is constituted by an outermost borosilicate glass layer on top of hafnia grains, and extends up to the un-oxidised bulk. The thickness of this multiphase oxide scale increases for higher testing temperatures (i.e. condition OX1). Due to the diminished viscosity for increasing temperatures, the external glass may flow laterally, and often forms an undulating pattern.

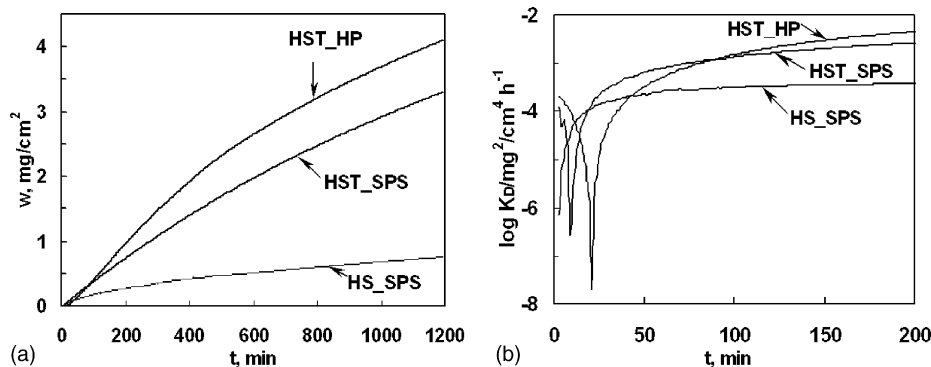


Fig. 8. Mass gain (w) vs. time (t) at 1450 °C for 20 h: the thermo-gravimetric curves (a); dummy parabolic rate constant K_D , $K_D = w^2/t$ (b).

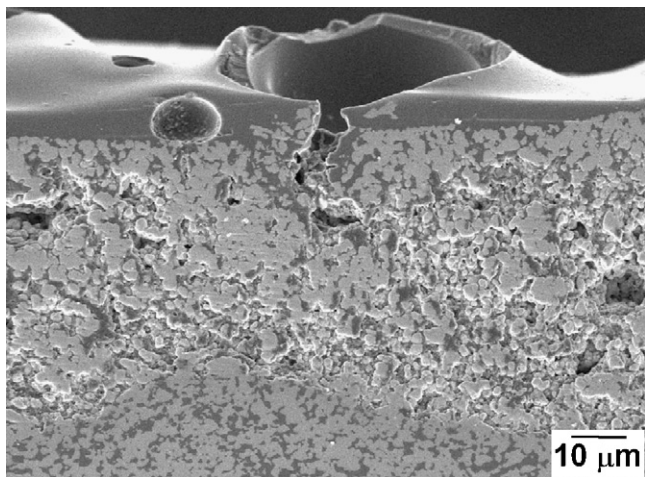
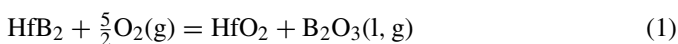


Fig. 9. SE-SEM micrograph from HST_HP, oxidised at 1450 °C for 20 h: a particular of the (polished) external oxide.

A thicker external glass coating locally implied a better protection against oxidation, and thus a reduced penetration of the corroded scale. The last note makes clear the fundamental contribution to the oxidation resistance from the borosilicate glass when it starts covering consistently the faces exposed to air.

The XRD analyses of the oxidised surfaces basically identified monoclinic hafnia. In fact, according to the following reaction,



mass gain is largely due to the oxidation of HfB₂ into HfO₂.

Regarding the samples oxidised at 1450 °C for 20 h (condition OX3), the multi-layered arrangement already described apart, a number of burst bubbles on surface or within the external glass was seen (Fig. 9). The boron oxide components firstly incorporated in the borosilicate glass were deemed to partially evolve outside as volatile species. The (Ta, Hf)-mixed carbides demonstrated to be stable at 1450 °C but transformed into some oxides when interacting with the incoming oxygen. The consequent evolution of gaseous CO, much more evident in HST_HP, might have contributed to originate bubbles in the external glassy coating.

According to the energy resolution, SEM-EDX analyses seem to indicate incorporated Ta atoms in the borosilicate glass and in the hafnia crystals. Small quantities of Ta in the external glass affected the resistance to oxidation: the mass gain of HS_SPS was lower than those of the TaSi₂-doped HST_SPS and HST_HP materials. It should be also taken into account that the oxygen diffusivity at high temperature through the hafnia crystals might have been enhanced by Ta atoms incorporated in the monoclinic hafnia lattice. However, a definitive assessment of this description by using SEM-EDX analyses is complicated by the overlap of the Ta Mα1 peak (1.71 keV) with the Hf Mα1 (1.645 keV) and Si Kα1 (1.74 keV) peaks, and must be conclusively confirmed by another analytical technique.

4. Discussion

4.1. Densification and microstructural texture

The comparison of the densification curves during SPS in Fig. 1 makes apparent the influence of the silicide additive on the densification behavior of HST_SPS. In addition, considering the pattern of the densification curves, the formation of a liquid phase from the added silicide most likely occurred. Within the temperature range of 1400–1800 °C, such a liquid medium was deemed to have favored not only rearrangements of the loose powder particles, but also more effective mass transfer through thermally activated diffusion mechanisms for increasing temperatures. The added silicide apart, other physical factors that contributed to complete densification of HST_SPS quickly were not only the rapid heat transfer, but mainly the contemporary application of a pulsing electric field and of an external pressure.

The benefits from the addition of TaSi₂ for densification can be reaffirmed in the HST_HP case. An amount of 20 vol% TaSi₂ added to an HfB₂ + 20 vol% SiC formulation demonstrated to lower significantly the sintering temperature (i.e. 1700 °C) necessary to achieve full density [8]. Undoped HfB₂-SiC powder mixtures on their own exhibit a sinterability considerably lower than that of an HfB₂-SiC-TaSi₂ mixture. Hot-pressing experiments on the HfB₂ + 20 vol% SiC system entailed temperatures and dwell times of 2000 °C and 2 h [8], or 2200 °C and 1 h [9] for achieving 97% relative density and full density, respectively.

The role of the SiC particulates should not be disregarded at all. In-air storage/processing of a metal diboride powder like HfB₂ or ZrB₂ are known to contaminate its particle surface with oxygen [3,4]. Such a contamination by oxygen has the effect of retarding, during any hot-consolidation treatments, those matter transfer mechanisms like boundary/volume diffusion responsible for a successful densification process in terms of maximum attainable density. The achievement of refined and pore-free microstructures herein presented emphasises the beneficial role SiC played in enhancing densification of strongly refractory HfB₂-SiC matrices. The depletion in the oxygen impurity via chemical interactions with SiC and, to some extent, with a Si-based liquid phase is indicated as the way through which the HfB₂ powder particles re-activated their own surface reactivity. Such a physical re-activation of the HfB₂ particles effects an increased boron activity due to the generation of higher Hf vacancy concentration. At the same time, the contemporary application of increasing temperatures, external pressure, and pulsing electric field (only for HST_SPS) favored grain boundary/lattice diffusion, and assisted densification usefully.

Even though the SPS process was faster than hot-pressing, the peak temperature of 2100 °C led to grain growth as well, and thus a more pronounced coarsening of the HfB₂ grains occurred in HST_SPS rather than in HST_HP. Compared to the HP process, the diboride matrix grew so promptly in short times during the SPS process that its coarsening seems to be controlled more by interface reactions rather than diffusion-controlled grain growth mechanisms.

The chemical interaction between TaSi_2 and SiC may help in explaining the appearance of a liquid phase, and the formation of (Ta–Hf) mixed carbides. The following reaction



is thermodynamically favored for temperatures exceeding the melting point of Si (i.e. 1420°C). Increasing temperature, a Si-based liquid phase very likely forms in suitable amounts for acting as lubricant for particles rearrangement. For the HST_HP material, which underwent sintering conditions closer to thermodynamic equilibrium, the moderate initial increase of the densification rate and its subsequent slowdown (Fig. 2) are interpreted as the rearrangement stage of a liquid-phase sintering. Abundance of Hf in the bulk and elevated temperatures represent further favorable conditions for the incorporation of Hf atoms in the newly formed carbides. In addition, more than for HST_SPS, graphite confinement to the sintering environment and longer processing times provided a stronger reducing component which enhanced the carbothermal reduction of Hf-oxides.

However, the investigated microstructures of the materials produced did not reveal certain traces of such a liquid phase. Thus occurrence, nature, role and evolution of this liquid phase still remain matter of reasoning. A conversion into SiC , thanks to the high temperatures in a carbon-rich sintering environment, most likely could have succeeded.

4.2. Thermo-mechanical properties

The room temperature (RT) strength of HST_HP took great advantage of the addition of a considerable amount of SiC . The incorporation of SiC implied the grain size refinement of the diboride matrix, which is key for improvement of the strength. Wuchina and co-workers reported as RT strength the value of 440 MPa for a monolithic HfB_2 modified with Hf + C, and hot-pressed at 2150°C [7]. The RT strength was partially retained at 1500°C , thanks to the inertness to degrade under an oxidising environment of the phases composing HST_HP. In addition, the external glassy layer which covers the specimen's faces exposed to air prevents more serious alteration of the microstructure, and

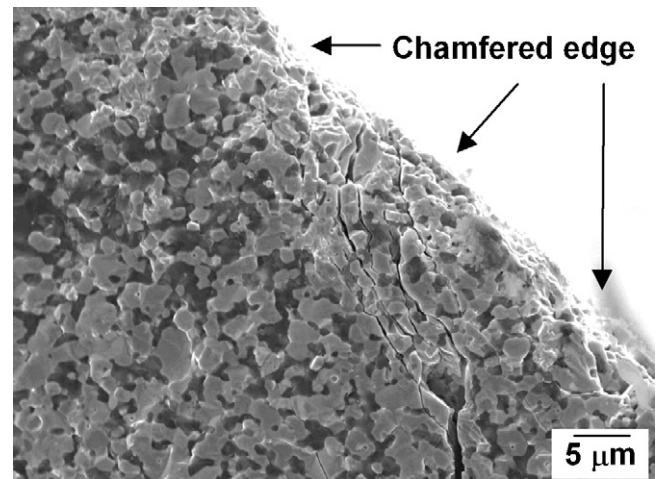


Fig. 10. SE-SEM micrograph from HST_SPS: the fractography of a broken specimen.

adds more protection to the inner bulk. The high-temperature strength after 1 h additional hold (Table 2) appears to fit this statement. According to previous experiments [10], the strength decrease at high temperature (in air) can be ascribed to the presence of the secondary carbides.

Concerning the strength behavior of HST_SPS, the RT strength showed a broad dispersion of data. The fractographic analyses for the lowest values ruled out the presence of intrinsic manufacturing defects, but more obviously revealed cracks extending from the chamfered edges into the bulk (Fig. 10). The premature failure was thus attributed to the coalescence of interconnecting micro-cracks, formerly generated by the mechanical machining. In contrast to HST_HP, which displayed a scattering of strength data typical for a ceramic, the cooling up to 1000°C in about 2 min might have induced a lot of unrelaxed thermal stresses, and thus an enhanced tendency to micro-cracking under external loads like the machining procedures.

Residual thermal stresses were already reported to come up at the HfB_2/SiC interfaces in consequence of the mismatch among elastic moduli, coefficients of thermal expansion and

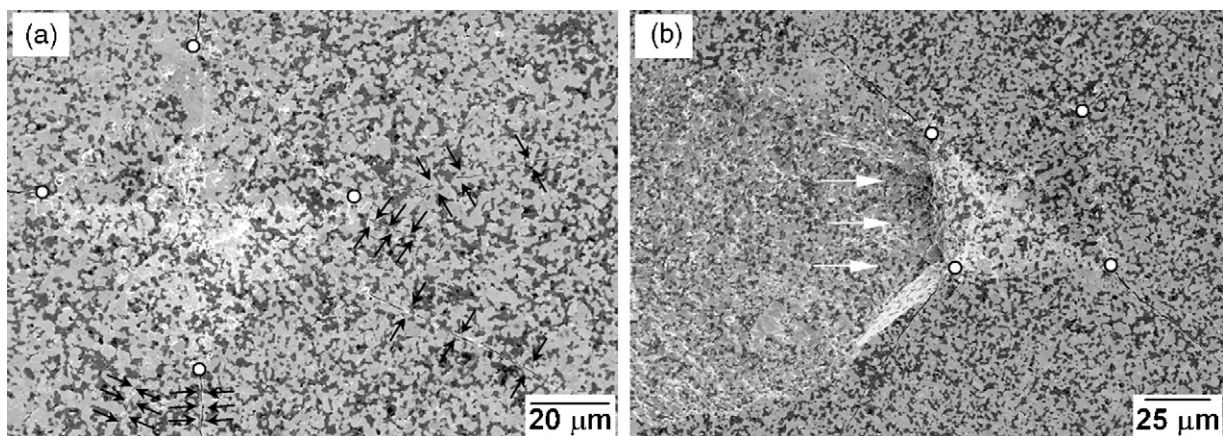


Fig. 11. SE-SEM micrographs from HST_SPS: branched cracks (black arrows, a) and a chipped area (white arrows) initiating from a Vickers indentation edge (b). Dots mark the indentation corners.

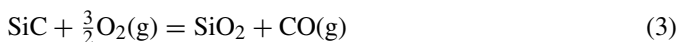
Poisson ratios of HfB_2 and SiC [10]. Vickers indentations on polished areas of HST_SPS probed representative volumes of the original microstructures but, differently from HST_HP, often did not induce the expected patterns of four cracks departing from the indentation corners (Fig. 11). This result was connected to the large thermal residual stresses whose emergence makes the mechanical machinability an issue. According to the condition OX2, the reduced dispersion of the RT strength for the oxidised specimens was associated to the formation of the borosilicate glass which, covering the machined faces of the specimens, sealed cracks and blunted their unfavorable impact for the strength measurement.

On the contrary, the increased fracture toughness compared to HST_HP seems to indicate that the as-sintered HST_SPS material took advantage of the very rapid cooling which prevented a controlled relaxation of the elastic strains. The freezing of such a thermal strained field in a particulate-reinforced ceramic–matrix composite very likely supported toughening mechanisms like thermal residual stress, crack deflection or crack pinning. The interaction between crack front and SiC particulates through the concomitant mechanisms already mentioned provided an overall benefit for fracture toughness.

4.3. The resistance to oxidation

The experimental tests (Figs. 7 and 8) showed limited oxidation resistance, even though, compared to the silicide-free HS_SPS formulation, the added TaSi_2 basically was not fully beneficial for improving the property considered. A similar behaviour was confirmed by Opila et al. [8].

As far as the thermo-gravimetric tests at 1450°C are concerned (condition OX3), the undulating change in the oxidation rate during heating discloses properly how the incorporated SiC enhances the resistance to oxidation of HfB_2 alone (Fig. 12). According to reaction 1, HfB_2 , once oxidised, yields HfO_2 and B_2O_3 . Silicon carbide, in accordance with the following reaction



reacts with oxygen and provides condensed silica (i.e. passive oxidation) which easily combines with the available B_2O_3 and forms a borosilicate glass. Such an oxidation product retards not

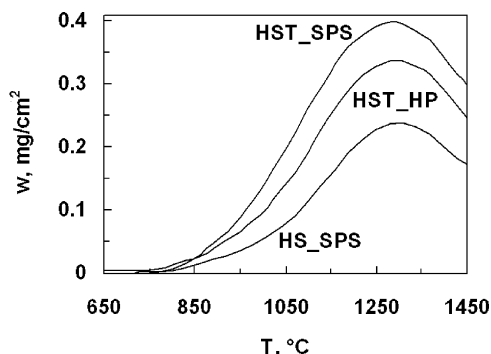


Fig. 12. Mass gain (w) vs. temperature (T) during heating up to 1450°C ($30^\circ\text{C}/\text{min}$).

only the loss of some boron oxides components (i.e. net mass loss from about 1300 up to 1450°C) but significant further inner diffusion of oxygen as well, giving more oxidation protection than HfO_2 alone.

Increasing temperatures up to 1650°C (condition OX1), the incorporated SiC continues providing oxidation protection and, excluded HST_SPS for temperatures above 1600°C , the experimental trends agree with oxidation-resistant parabolic kinetics.

It is the author's considered opinion that at 1450°C , the lower resistance to oxidation (Figs. 8 and 12), compared to HS_SPS, can be ascribed to less protective borosilicate glasses enriched by Ta. On the one hand, the cation Ta is known for ionic field strength lower than that of Hf [11]. It thus acts as a glass network-modifier, and lowers the ability of the surface glass itself to retard the oxygen diffusion, due to a decreased viscosity. On the other hand, the reaction scale morphology revealed that the external HfO_2 skeleton provides a framework for the glass to be retained, and not removed by shear forces, mitigating the effects of oxidation. It should also be noted that the temperature of 1450°C is next to the inferior bound of the temperature range within which the as-fired specimens may fully benefit by the protective capabilities of the external oxide scale. If the permeability to oxygen of HfO_2 (and hence the overall resistance to oxidation) might be influenced by incorporated Ta atoms is still object of consideration. The effective vacancy concentration in the Ta-modified HfO_2 seems to be the key factor.

5. Summary

The powder mixture $\text{HfB}_2 + 30 \text{ vol}\% \text{ SiC} + 2 \text{ vol}\% \text{ TaSi}_2$ was fully densified by spark plasma sintering and hot-pressing. The microstructures consist of micrometric diboride grains, and SiC evenly distributed. Few secondary phases were found: HfO_2 and (Ta, Hf)-mixed carbides. Regardless of the sintering technique used, both SiC and TaSi_2 were recognised as activators of an enhanced sinterability of HfB_2 .

The thermo-mechanical properties took full advantage of the addition of SiC . Elastic moduli above 490 GPa and thermal expansion of about $7 \times 10^{-6}/^\circ\text{C}$ were measured. The flexural strengths at room temperature and 1500°C (in air) of the hot-pressed ceramic were 665 ± 75 and $480 \pm 30 \text{ MPa}$, respectively.

The steep cooling up to 1000°C in about 2 min during spark plasma sintering caused large unreleased thermal stresses, and enhanced the tendency of the HfB_2 – SiC system to micro-cracking. Such a feature sets the mechanical machining as an issue: machining-induced flaws rather than fabrication defects degraded strength. On the contrary, the thermal residual stress field in the spark plasma sintered material effected an increased fracture toughness, compared to the hot-pressed one.

Both the ceramics proved to endure in-air oxidising conditions from 1450 up to 1650°C well: effective protection against oxidation was achieved through the coverage of a borosilicate glass. During 20 h exposure at 1450°C in air, oxidation kinetics were basically decelerating, but deviated from purely parabolic trends: compared to a composition free of network modifiers,

the external borosilicate glass modified by Ta atoms increased its own permeability to oxygen.

Acknowledgements

The author wishes to acknowledge the support of his colleague A. Balbo (oxidation tests), C. Melandri (mechanical tests), and FCT Systeme GmbH, Rauenstein, Germany (SPS experiments). Insightful discussion on the mechanical properties was acknowledged to S. Guicciardi as well.

References

- [1] D.M. Van Wie, D.G. Drewry Jr., D.E. King, C.M. Hudson, *J. Mater. Sci.* 39 (2004) 5915–5924.
- [2] M.M. Opeka, I.G. Talmy, J.A. Zaykoski, *J. Mater. Sci.* 39 (2004) 5887–5904.
- [3] F. Monteverde, S. Guicciardi, A. Bellosi, *Mater. Sci. Eng. A346* (2003) 310–319.
- [4] F. Monteverde, A. Bellosi, *J. Mater. Res.* 19 (12) (2004) 3576–3585.
- [5] A.L. Chamberlain, W.G. Fahrenholtz, G.E. Hilmas, *J. Am. Ceram. Soc.* 87 (6) (2004) 1170–1172.
- [6] M. Nygren, Z. Shen, *Solid State Sci.* 5 (2003) 125–131.
- [7] E. Wuchina, M. Opeka, S. Causey, K. Buesking, J. Spain, A. Cull, J. Roubort, F. Guitierrez-Mora, *J. Mater. Sci.* 39 (2004) 5939–5949.
- [8] E. Opila, S. Levine, J. Lorincz, *J. Mater. Sci.* 39 (2004) 5969–5977.
- [9] M. Gasch, D. Ellerby, E. Irby, S. Beckman, M. Gusman, S. Johnson, *J. Mater. Sci.* 39 (2004) 5925–5937.
- [10] F. Monteverde, *Compos. Sci. Technol.* 65 (11–12) (2005) 1869–1879.
- [11] W. Vogel, *Structure and Crystallization of Glasses*, Pergamon Press, 1971, p.17.